

Analytical model of hyperspectral system performance*

John P. Kerekes, Jerrold E. Baum, Kristine E. Farrar

Sensor System Applications Group
Lincoln Laboratory
Massachusetts Institute of Technology
244 Wood St., Lexington, MA 02420-9185

ABSTRACT

In support of hyperspectral sensor system design and parameter tradeoff investigations, an analytical end-to-end remote sensing system performance forecasting model is being developed. The model uses statistical descriptions of class reflectances in a scene and propagates them through the effects of the atmosphere, the sensor, and any processing transformations. A resultant system performance metric is then calculated based on these propagated statistics. The model divides a remote sensing system into three main components: the scene, the sensor, and the processing algorithms. Scene effects modeled include the solar illumination, atmospheric transmittance, shade effects, adjacency effects, and overcast clouds. Sensor effects modeled include the following radiometric noise sources: shot noise, thermal noise, detector readout noise, quantization noise, and relative calibration error. The processing component includes atmospheric compensation, various linear transformations, and a spectral matched filter used to obtain detection probabilities. This model has been developed for the HYDICE airborne imaging spectrometer covering the reflective solar spectral region from 0.4 to 2.5 μm . The paper presents the theory and operation of the model, as well as provides the results of validation studies comparing the model predictions to results obtained using HYDICE data. An example parameter trade study is also included to show the utility of the model for system design and operation applications.

Keywords: hyperspectral system modeling, sensor parameter tradeoffs

1. INTRODUCTION

1.1 Background

Interest has been growing in the use of hyperspectral imaging systems (electro-optical sensors with moderate to high spatial resolution and hundreds of narrow, contiguous spectral channels) for a number of applications. Experiments with nadir-viewing airborne sensors have shown the feasibility of these systems to find and identify subpixel, or unresolved, objects through the use of the spectral information. However, there are a number of questions regarding the robustness of spectral imaging technology to environmental conditions and object/background variations. It is neither practical nor affordable to conduct field experiments to explore the robustness for all expected situations, and therefore the quantitative exploration of these questions falls best to the realm of modeling.

Models and simulation can occur at a range of fidelity and complexity to answer various questions related to the performance of spectral imaging technology. Detailed first-principles physics-based simulations can take a well-defined scene and predict what a given sensor would see. This approach is very useful to provide known data sets for algorithm development as well as to provide a phenomenological basis for explaining imagery collected by real sensors. However, these simulations can be time consuming to set up and computationally demanding, thus limiting the number of different scenes and sensor designs that can be considered.

Another approach is to rely on statistical descriptions of the scene and sensor effects and predict system performance using analytical equations. The potential loss of detail in this approach is offset by reduced run-time and complexity, thus allowing a large number of parameter trades to be conducted and sensitivities studied.

* This work was sponsored by the Department of Defense under Air Force contract F19628-95-C-0002. Opinions, interpretations, conclusions, and recommendations are those of the authors and not necessarily endorsed by the United States Air Force.

The work described in this paper takes this analytical approach and adapts a previously developed model¹ to subpixel object detection and spectral characterization applications.

1.2 Model objective

Lincoln Laboratory is developing an analytical model to quantitatively forecast the ability of a hyperspectral remote sensing system to perform a given task. The Forecasting and Analysis of Spectroradiometric System Performance (FASSP) model considers the end-to-end remote sensing system process, including the scene to be imaged, the spectroradiometric sensor, and the processing algorithms used to derive a given performance metric. The model is being designed to run quickly and robustly, and to forecast not only the expected performance metric, but also the relative contributions of diverse system components and parameters. This paper will focus on the performance forecasting application of the model, as the relative contribution mode was discussed in a previous work².

The applications of this model include: 1) performing parameter trade studies during the sensor design phase, 2) examining sensitivities in object detection applications to environmental, scene background, and object characteristics, and 3) serving as a collection operations tool to optimize observation parameters for a given data collection. The model is also useful for exploring the performance of spectral imaging technology to provide a quantitative basis for programmatic decisions.

1.3 Paper overview

The next section describes the theory behind the modeling approach used in FASSP. Section 3 briefly discusses the implementation and use of the model. Section 4 covers the initial validation of the model by comparison to results obtained using existing airborne sensor data and includes the scene radiance statistics, detection operator statistics, and performance predictions. Section 5 presents an example model result to show capabilities of FASSP. Finally, the model is summarized and its future is discussed in Section 6.

2. MODEL THEORY

2.1 Model overview

The FASSP model propagates the means and covariances of the spectral reflectances of objects (targets) and backgrounds through the effects of the atmosphere, the sensor, and algorithmic transformations. The final output of the model is a system performance metric. It covers spectral imaging sensors working in the reflective solar spectral region and applications of target detection (using a known spectral signature) or spectral reflectance characterization.

2.2 Scene model

FASSP considers a scene to consist of one, or more, background classes and a target class. The user supplies the proportion of the scene filled by each background class and the fraction of a pixel occupied by the target class. Each class (background and target) is described by its first- and second-order spectral reflectance statistics (mean and covariance). Weighted combinations of these reflectance vectors, along with descriptions of the atmosphere and the observation geometry, are transformed by the atmospheric code MODTRAN into surface-reflected and path-scattered radiances. These radiances are then combined to produce the mean and covariance statistics of the spectral radiance at the input aperture of a spectral imaging sensor. The notional scene geometry, reflectance inputs, transformations, and at-sensor radiance are detailed below.

2.2.1 Notional scene geometry and subpixel target model

FASSP 1.0 assumes a simple area-weighting model for a subpixel target within a scene that contains one or more distinct background classes. Each of the M background classes occupies a fraction f_m of the scene, with the constraint the fractions sum to 1. The subpixel target is considered to be embedded within one of these classes, denoted m^* . It is important to note that FASSP does not actually simulate a specific spatial layout, but rather accounts for the effects of the multiple background classes through an area-weighting process.

A simple linear model is assumed for the notional target class pixel. The subpixel fraction f_T ($0 < f_T \leq 1$) defines the fractional area of the target class pixel occupied by the target with a direct line-of-sight to the sensor. Parts of the target occluded by

the background are accounted for in the background fraction. The fraction of the target in shadow, f_S , ($0 \leq f_S \leq 1$) is illuminated only by diffuse sky irradiance, assuming the object casting the shadow is opaque. In cases where $f_S > 0$, the fractional amount of the sky's full hemisphere visible from the target, f_{sky} , ($0 < f_{sky} \leq 1$) must be specified. This allows for a situation where the full hemisphere of downwelling sky irradiance may be partially blocked, (e.g., a target on the ground down between tall trees), and only a fraction of the sky is visible from the target. In these cases, the amount of diffuse, or sky, radiance is reduced proportionally by f_{sky} .

2.2.2 Input reflectance statistics

The target and background spectral reflectance statistics are computed externally and provided as inputs to the FASSP model. They may be derived from airborne spectrometer imagery converted to reflectance, field spectrometers, laboratory measurements, or physics-based simulations. For each class, the input statistics consist of a K -dimensional spectral mean reflectance vector ρ and a $K \times K$ reflectance spectral covariance matrix Σ_ρ .

The model assumes that the reflectance distribution of each class, background or target, is unimodal. Thus, the data used to compute the statistics must be carefully screened, through spectral clustering or histogram techniques, to ensure they form a cluster around a single mean point in the K -dimensional space. In some cases, a single terrain category will need to be separated into multiple reflectance classes to ensure each class is unimodal. For example, the single category 'grass' may need to be split into 'dry grass' and 'healthy grass' classes, each with a different mean reflectance.

Also, the model considers the reflectance vectors to be hemispherical reflectance factors for completely diffuse surfaces³. FASSP does not include BRDF effects.

2.2.3 Atmospheric radiance and transmittance - MODTRAN

The FASSP model uses the Air Force Research Laboratory code MODTRAN⁴ for the solar illumination and atmospheric effects. A number of calls are made to the code to calculate the various radiance vectors used to transform the reflectance statistics to radiance statistics. For convenience in the current version of the software, the sensor channel spectral response functions are convolved with the spectral radiances immediately after each MODTRAN run is completed. Thus, the spectral radiance vectors at the output of the scene model section have the same dimensionality as the sensor.

2.2.4 Mean spectral radiance[#]

Background Classes. A separate call to MODTRAN is made for each of the M background classes, as well as one for the scene average case. The total mean spectral radiance for each case is calculated as shown in equations (1) and (2) by the sum of $L_S(\rho)$, the total surface reflected radiance for a mean surface reflectance ρ , and $L_P(\rho_{ave})$, the scattered path radiance using a scene average for the surface albedo. This formulation for the path radiance accounts for the "adjacency effect" and is discussed at the end of this section.

$$L_{Bm} = L_S(\rho_m) + L_P(\rho_{ave}) \quad (1)$$

$$L_{Bave} = L_S(\rho_{ave}) + L_P(\rho_{ave}) \quad (2)$$

The scene average reflectance, ρ_{ave} , is calculated using the scene fractions f_m as in equation (3).

$$\rho_{ave} = \sum_{m=1}^M f_m \rho_m \quad (3)$$

Target in Open. When the target is in the open (no shadows present) the mean spectral radiance for the target class is calculated as shown in equation (4).

$$\tilde{L}_T = L_S(\tilde{\rho}_T) + L_P(\rho_{ave}) \quad (4)$$

[#] Note: all radiance calculations are performed as a function of wavelength but for clarity in presentation the subscript λ has been dropped.

The surface albedo used in the MODTRAN call to generate the first term of equation (4) is calculated as in equation (5). The weighted sum of the target class mean reflectance and the background class m mean reflectance implements the linear model described above in section 2.2.1.

$$\tilde{\rho}_T = f_T \rho_T + (1 - f_T) \rho_m. \quad (5)$$

Target in Shadow. When the target is in full or partial shadow, the calculation is done slightly differently to handle the various sources of illumination. Equation (6) shows the mean target spectral radiance for this case.

$$\begin{aligned} \tilde{L}_T = & f_T \left[(1 - f_S) L_{SD}(\rho_T) + f_{sky} (L_S(\rho_T) - L_{SD}(\rho_T)) \right] \\ & + (1 - f_T) L_S(\rho_m) + L_P(\rho_{ave}) \end{aligned} \quad (6)$$

L_{SD} is the direct (from the sun) ground reflected radiance, whereas L_S is the total (including sky irradiance) ground reflected radiance. Thus, the contribution from the sky irradiance is assumed to be the difference $L_S - L_{SD}$.

Path Radiance Calculation. For all mean spectral radiance calculations, the path-scattered contribution L_P is calculated using the scene fractional area-weighted average reflectance ρ_{ave} . (Note that when MODTRAN is run with the multiple scattering option on, the atmospheric scattered path radiance term depends on the surface albedo.) This approach accounts for the ‘‘adjacency effect’’, which is the scattering of nearby surface reflected radiance into the sensor’s instantaneous field-of-view (IFOV). The assumption here is that the scattering scale of the effect covers the entire scene being collected. Studies have shown this effect can occur out to several hundred meters⁵, typical of the scenes considered by the model.

2.2.5 Spectral radiance covariance

The transformation of the spectral reflectance covariance statistics to spectral radiance covariance statistics follows the same linear atmospheric model assumed in the mean calculations. The idea behind the transformation is to interpolate spectral radiances calculated for surface albedos equal to 0 and 1 using the entries of the reflectance covariances. The following diagonal matrices are used in these transformations, with the described vectors along the diagonals and zeros elsewhere.

Λ_{LS1}	=	total surface reflected spectral radiance for surface albedo = 1.
Λ_{LD1}	=	direct surface reflected spectral radiance for surface albedo = 1.
Λ_{LP1}	=	atmospheric path scattered spectral radiance for surface albedo = 1.
Λ_{LP0}	=	atmospheric path scattered spectral radiance for surface albedo = 0.

Background Classes. The background spectral radiance covariance matrices for each of the M background classes and the scene average are calculated as shown in equations (7) and (8). G_{CB} is a user-specified scalar used to study the effect of scaling the background covariance matrices.

$$\begin{aligned} \Sigma_{LBm} = & \Lambda_{LS1} G_{CB} \Sigma_{\rho Bm} \Lambda_{LS1} + \\ & [\Lambda_{LP1} - \Lambda_{LP0}] G_{CB} \Sigma_{\rho Bave} [\Lambda_{LP1} - \Lambda_{LP0}] \end{aligned} \quad (7)$$

$$\begin{aligned} \Sigma_{LBave} = & \Lambda_{LS1} G_{CB} \Sigma_{\rho Bave} \Lambda_{LS1} + \\ & [\Lambda_{LP1} - \Lambda_{LP0}] G_{CB} \Sigma_{\rho Bave} [\Lambda_{LP1} - \Lambda_{LP0}] \end{aligned} \quad (8)$$

Target in Open. The target class spectral radiance covariance matrix is calculated using the total surface reflected radiance output from MODTRAN as shown in equation (9). G_{CT} is similar to G_{CB} , defined above, but for the target class.

$$\begin{aligned} \Sigma_{LT} = & f_T^2 \Lambda_{LS1} G_{CT} \Sigma_{\rho T} \Lambda_{LS1} + \\ & (1 - f_T)^2 \Lambda_{LS1} G_{CB} \Sigma_{\rho Bm} \Lambda_{LS1} + \\ & [\Lambda_{LP1} - \Lambda_{LP0}] G_{CB} \Sigma_{\rho Bave} [\Lambda_{LP1} - \Lambda_{LP0}] \end{aligned} \quad (9)$$

Target in Shadow. As in the mean case, the shadowed target covariance calculation separates out the sky, or diffuse, irradiance contribution as shown in equation (10).

$$\begin{aligned} \Sigma_{LT} = & f_T^2 \left\{ (1 - f_S)^2 \Lambda_{LD1} G_{CT} \Sigma_{\rho T} \Lambda_{LD1} + \right. \\ & \left. f_{sky}^2 [\Lambda_{LS1} - \Lambda_{LD1}] G_{CT} \Sigma_{\rho T} [\Lambda_{LS1} - \Lambda_{LD1}] \right\} + \\ & (1 - f_T)^2 \Lambda_{LS1} G_{CB} \Sigma_{\rho Bm} \Lambda_{LS1} + \\ & [\Lambda_{LP1} - \Lambda_{LP0}] G_{CB} \Sigma_{\rho Bave} [\Lambda_{LP1} - \Lambda_{LP0}] \end{aligned} \quad (10)$$

2.3 Sensor model

The sensor model takes the spectral radiance mean and covariance statistics for the various ground classes and applies sensor effects to produce signal mean and covariance statistics that describe the scene as imaged by an imaging spectrometer. The sensor model in this version is relatively simple, including a limited number of radiometric noise sources, with no spatial or spectral sources of error included. Also, as was noted earlier, the channel spectral response of the sensor is applied during the input radiance calculations described in the previous section. Currently, the only sensor included in FASSP is HYDICE⁶ and the spectral channels are fixed, but other sensor types can be considered by varying certain sensor parameters.

2.3.1 Electronic gain

The mean signal level in the sensor model can be adjusted by a gain parameter, G_S , which scales the signal to study the impact of changing the sensor's electronic gain. The mean levels from the sensor component model are calculated as shown in equation (11), where L_i is the mean signal radiance for the different classes (indexed by subscript i) being tracked through the model. Note that the spectral covariance matrices are also affected by the gain parameter as shown in equation (12).

$$S_i = G_S L_i \quad (11)$$

$$\Sigma_{S_i} = G_S^2 \Sigma_{L_i} \quad (12)$$

2.3.2 Radiometric noise

Radiometric noise processes are modeled by their effects on the diagonal entries of the spectral covariance matrices. Off-diagonal entries are not affected as the assumption is that there is no channel-to-channel correlation in the noise processes.

The radiometric noise sources come from the detector noise processes and include the photon (shot) noise, thermal noise, and multiplexer/readout noise. Since some detector parameters are often specified in terms of electrons in CCD focal plane arrays, the noise terms are summed in a root sum squared sense in that domain before being converted to noise equivalent spectral radiance. To calculate the photon noise term σ_{np} , the input radiance is converted to electrons and the square root taken as shown in equation (13). Note that this calculation is done for each signal being tracked through the model and for each spectral channel separately.

$$\sigma_{np} = \sqrt{L \times A\Omega \times \tau \times \eta \times t \times \Delta\lambda \times C_U \times \lambda / (h \times c)} \quad (13)$$

where,

L	= input spectral radiance (mW/(cm ² -sr- μ m))
$A\Omega$	= system throughput (cm ² -sr)
τ	= optical transmittance
η	= quantum efficiency
t	= integration time (sec)
$\Delta\lambda$	= spectral channel bandwidth (μ m)
λ	= spectral channel central wavelength (μ m)
h	= Planck's constant = 6.63×10^{-34} J-sec
c	= the speed of light = 3.0×10^8 m/sec
C_U	= unit conversion constant = 10^{-9} .

The total detector noise (in electrons) is then calculated by the root sum square of the photon noise σ_{np} , the thermal noise σ_{nt} , and the multiplexer/readout noise σ_{nm} as follows.

$$\sigma_n = \sqrt{\sigma_{np}^2 + \sigma_{nt}^2 + \sigma_{nm}^2} \quad (14)$$

The total detector noise σ_n (in electrons) is then converted back to noise equivalent spectral radiance σ_{Ln} and scaled by a user-specified noise factor G_n before being added to the diagonal entries of the spectral covariance matrices as shown in equation (15) for each spectral channel l .

$$\Sigma_{S_i}^n(l, l) = \Sigma_{S_i}(l, l) + G_n^2 \sigma_{Ln, l}^2 \quad (15)$$

2.3.3 Relative calibration error

The next noise source considered is relative calibration error C_R . This error is assumed to be uncorrelated between spectral channels, with a standard deviation σ_{CR} proportional to the mean signal level. Thus, for each signal, this noise source is added as shown in equation (16).

$$\Sigma_{S_i}^{n+c}(l, l) = \Sigma_{S_i}^n(l, l) + [S_i(l) \times (C_R / 100)]^2 \quad (16)$$

2.3.4 Quantization noise and data link errors

The last two noise sources are the quantization noise in the analog-to-digital conversion and bit errors in the communications or data recording system. These both depend upon the electronic gain factors and the assumed dynamic range of the sensor L_{max} . The quantization error variance is calculated as shown in equation (17).

$$\sigma_{nq}^2 = \frac{1}{12} \left(\frac{L_{max} / G_s}{2^Q - 1} \right)^2 \quad (17)$$

The effect of bit errors in the data link (or on-board storage) is derived as follows. It is assumed that bit errors are uniformly distributed across the data word and could be of either sign. Thus, for Q bits, the error will take on one of $2Q$ values, $\pm 2^k$ for $k=0, \dots, Q-1$, with equal probability of $1/(2Q)$. The noise variance, σ_{nBe}^2 , due to a bit error rate of B_e is shown in equation (18).

$$\sigma_{nBe}^2 = \frac{B_e}{Q} \sum_{q=0}^{Q-1} \left(2^q \frac{L_{max} / G_s}{2^Q - 1} \right)^2 \quad (18)$$

These last two noise terms σ_{nq}^2 and σ_{nBe}^2 are added to the diagonal entries of the spectral covariance matrices in a similar manner as was the calibration error in equation (16).

2.3.5 Signal-to-noise ratio

The sensor signal-to-noise ratio (SNR) is calculated within the model as the ratio between the mean signal and the square root of the sum of the noise variance terms as shown in equation (19), where i is either the target or one of the background classes.

$$SNR_i = \frac{S_i}{\sqrt{\sigma_{Lni}^2 + \sigma_{CR}^2 + \sigma_{nq}^2 + \sigma_{nBe}^2}} \quad (19)$$

2.4 Processing model

2.4.1 Atmospheric compensation and spectral characterization accuracy

In this initial version of FASSP, atmospheric compensation is accomplished by using low and high reflectance surrogate calibration panels and computing the slope m and offset o with a two-point linear fit between the mean panel signal and the known reflectance. This models the widely used empirical line method (ELM) for atmospheric compensation.

The slopes and offsets are applied to the mean signal and covariance matrices of the various target and background classes to compute the retrieved (or estimated) class reflectance mean $\hat{\rho}$ and covariance $\hat{\Sigma}$ statistics. The spectral characterization accuracy is described by the mean difference, SC_{bias} , between the retrieved surface reflectance of the target and the initial known reflectance, and by the standard deviation, σ_{SC} , of the difference for each spectral channel l , as in equations (20) and (21).

$$SC_{bias}(l) = \hat{\rho}(l) - \rho(l) \quad (20)$$

$$\sigma_{SC}(l) = \sqrt{\hat{\sigma}_{\rho}^2(l,l) - \sigma_{\rho}^2(l,l)} \quad (21)$$

2.4.2 Feature selection

In FASSP 1.0 several options are available for extracting a reduced dimensionality feature vector from the signal vector. These include: 1) all channels within contiguous region(s), (e.g., to avoid water vapor absorption spectral regions), 2) principle components, or 3) band averaging to simulate multispectral channels. All options are implemented as a linear transformation using a feature selection matrix Ψ . This matrix is applied to both the mean vectors and the covariance matrices in the retrieved reflectance domain (if atmospheric compensation was performed) or in the signal domain directly on the statistics output by the sensor model.

$$F_i = \Psi^T X_i \quad (22)$$

$$\Sigma_{F_i} = \Psi^T \Sigma_{X_i} \Psi \quad (23)$$

In equations (22) and (23), the variable X refers to the signal type (retrieved reflectance or sensor signal) and the index i refers to the various target and background classes.

2.4.3 Performance metrics

In FASSP 1.0, two algorithms are available to determine a performance metric for a given scenario: 1) a version of Constrained Energy Minimization (CEM)⁷ and 2) Total Error. CEM can be used to predict P_D/P_{FA} curves in the Forecast Mode, while Total Error approximates the sum of false alarm and missed detection probabilities and is used as a metric to measure relative impacts on performance during parameter trade studies.

Constrained Energy Minimization (CEM) The CEM operator uses a known target “signature” and an estimate of the background spectral covariance to minimize the energy from the background and to emphasize the desired target. In the FASSP implementation, the known “signature” is actually the unmodified original target mean reflectance used at the input to the model. The operator w is formed as shown in equation (24), where the subscript F indicates the signal means and covariances have been transformed to the desired feature space using equations (22) and (23).

$$w = \frac{\hat{\Sigma}_{\rho_{FBave}}^{-1} (\rho_{FT} - \hat{\rho}_{FBave})}{(\rho_{FT} - \hat{\rho}_{FBave})^T \hat{\Sigma}_{\rho_{FBave}}^{-1} (\rho_{FT} - \hat{\rho}_{FBave})} \quad (24)$$

This operator w is then used to transform the means and covariances from the feature space to a scalar test statistic with mean θ and variance σ_{θ}^2 , from which the P_D/P_{FA} curve can be calculated. The operator is applied to the combined target/background features and to the features of each of the background classes as shown in the following set of equations.

$$\theta_T = w^T (\hat{\rho}_{FT} - \hat{\rho}_{FBave}) \quad (25)$$

$$\theta_{Bm} = w^T (\hat{\rho}_{FBm} - \hat{\rho}_{FBave}) \quad \text{for } m = 1 \dots M \quad (26)$$

$$\sigma_{\theta_T}^2 = w^T \hat{\Sigma}_{\rho_{FT}} w \quad (27)$$

$$\sigma_{\theta_{Bm}}^2 = w^T \hat{\Sigma}_{\rho_{FBm}} w \quad \text{for } m = 1 \dots M \quad (28)$$

The probability of detection P_{Dm} (computed separately for each background class m) is then computed for a specified probability of false alarm P_{FA} , using a Gaussian assumption for the test statistic output by the CEM operator. This

assumption is loosely justified by the Central Limit Theorem since the operator is really just the summation of a large number of random variables. Section 4 discusses this assumption further. The threshold h_m is determined from the desired probability of false alarm and mean θ_{Bm} and variance $\sigma_{\theta_{Bm}}^2$ for each background class m . The function Φ^{-1} returns the cutoff value such that the area under the standard normal curve to the right of the cutoff is equal to the argument of the function.

$$h_m = \theta_{Bm} + \sigma_{\theta_{Bm}} \Phi^{-1}(P_{FA}) \quad (29)$$

$$P_{Dm} = \frac{1}{\sigma_{\theta_T} \sqrt{2\pi}} \int_{h_m}^{\infty} \exp\left[-\frac{(x - \theta_T)^2}{2\sigma_{\theta_T}^2}\right] dx \quad (30)$$

For scenarios with multiple backgrounds, the threshold h^* yielding the minimum P_D is used to recompute the P_{FA} 's for the other classes. These new P_{FA} 's are then summed using the background class area fractions f_m to yield a combined P_{FA} . The combined P_D is simply the minimum P_{Dm} .

$$P_{FA} = \sum_{m=1}^M f_m P_{FAm}(h^*) \quad (31)$$

$$P_D = \min P_{Dm} \quad (32)$$

Total Error. This metric approximates the total error P_e (i.e., the overlap between multivariate distributions) in a two-class equal *a priori* probability case⁸ as shown in equation (33).

$$P_e \approx \frac{1}{2}(1 - P_D) + \frac{1}{2} P_{FA} \quad (33)$$

While P_e does not distinguish between errors due to false alarms or missed detections, it does provide a single scalar metric that can be used for relative performance comparisons. It is normally used within FASSP for the System Analysis Mode which calculates the relative contribution to system error from the various system parameters using P_e as a metric. P_e is calculated using the standard normal error function and the Bhattacharyya distance B ,

$$P_e = \frac{1}{\sqrt{2\pi}} \int_{\sqrt{2B}}^{\infty} \exp\left(-\frac{x^2}{2}\right) dx \quad (34)$$

where,

$$B = \frac{1}{8}(F_T - F_B)^T \left(\frac{\Sigma_{FT} + \Sigma_{FB}}{2} \right)^{-1} (F_T - F_B) + \frac{1}{2} \ln \frac{|\Sigma_{FT} + \Sigma_{FB}|}{\sqrt{|\Sigma_{FT}| |\Sigma_{FB}|}} \quad (35)$$

3. OPERATION

The FASSP model has been implemented in the Interactive Data Language (IDL) of Research Systems Incorporated, taking advantage of the integrated Graphical User Interface (GUI) and plotting capabilities, as well as the portability between computing platforms.

The scene, sensor, and processing parameters are specified through a scenario parameter file loaded into FASSP. These values may be modified through the GUI. A software control executive allows automatic trade studies to be conducted for a number of parameters. A typical parameter trade study takes only a few minutes on a UNIX workstation.

4. VALIDATION

Validation of the FASSP model has been explored for a number of scene types. The example case shown below is typical of the results obtained. In this example, the means and standard deviations of the spectral radiances, the distributions of the detection statistic, and the final performance predictions of detection probabilities are all considered. The example case uses data collected by HYDICE over a test site at the Aberdeen Proving Grounds in August, 1995.

4.1 Scene radiometry

An important aspect of the validation process is a comparison between the spectral radiance as measured by a real sensor to that predicted by the model for a scene as similar as possible. While it is recognized discrepancies may occur due to a number of reasons outside of the model (sensor calibration errors, unknown scene parameters, etc.), similar results give confidence that the model is working reasonably well.

This case compared the measured and predicted radiance statistics of a man-made object deployed on an open grassy field. The data-derived mean and standard deviation, shown in Figure 1, were calculated from Run 07 of a HYDICE data collection on August 24, 1995. To model this case, input parameters for FASSP, such as the solar zenith angle and other atmospheric conditions, were chosen to be as similar as possible to the actual scene conditions. In addition, to provide independent data to the model, the input spectral reflectance statistics were derived by applying ELM to data from an earlier HYDICE run.

The mean spectral radiance comparison shown in Figure 1a is very good and generally within 5% -10%, which is about the absolute accuracy of the sensor and the MODTRAN model used for the atmospheric effects.

The comparison of the standard deviation of spectral radiance shown in Figure 1b shows a greater difference between the model prediction and the actual data, but still within 25-30%. This difference may partly be explained by the different spatial resolutions of the data used to derive the reflectances. The data used by the model for the reflectance statistics (Run 05) were at a resolution of ~0.75 meters, while the Run 07 HYDICE radiance data used for comparison was ~1.5 meters. It has been observed that higher spatial resolution often leads to greater variance in the spectral domain. The results of Figure 1b are consistent with that observation since the model used the higher spatial resolution reflectances and predicts a greater standard deviation than seen in the data.

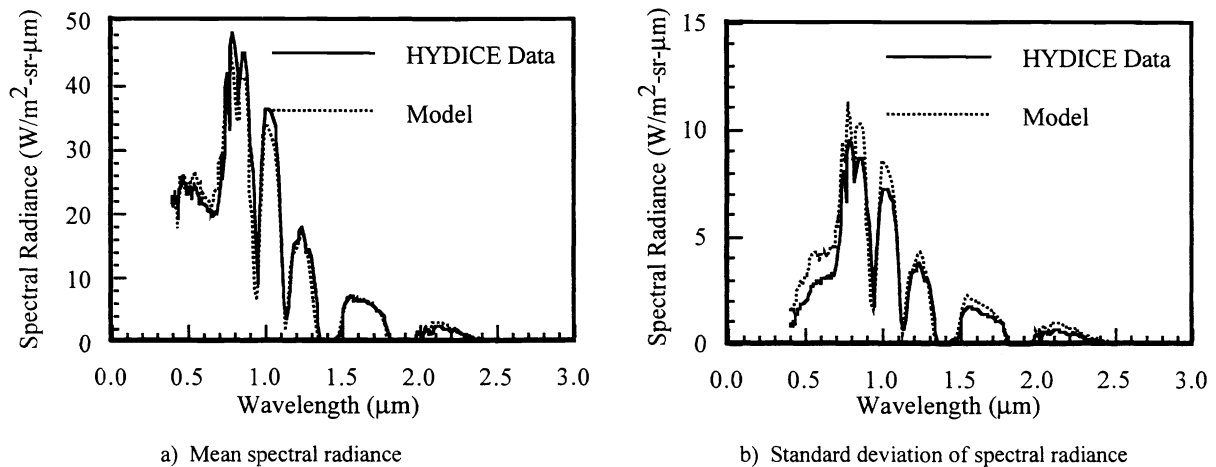


Figure 1. Radiance comparison for man-made object in HYDICE Run 07, 24 August 1995.

4.2 Detection statistic

As an independent check on the CEM detection statistic distributions, reflectance statistics over an area of the forest and the man-made test object were derived from Run 05 and used to forecast performance for Run 07. The HYDICE data from Run 07 were analyzed using CEM and the histograms (empirically derived probability density functions) were computed over the forest and the test object.

Figure 2 shows a graphical comparison of the density functions while Table 1 presents the quantitative results. The solid lines in Figure 2 are the empirical estimates of the probability density function of the CEM output value derived from the HYDICE data, while the dashed lines are Gaussian curves with a mean and standard deviation as predicted by the FASSP model using the independent reflectance data. The shapes of the empirically derived density functions in Figure 2 qualitatively confirm the model assumption that the CEM test statistics are Gaussian, although the limited number of samples for the test object distort the curve. Table 1 shows the quantitative comparisons of the means and standard deviations of the CEM output value with a good match achieved between the empirical result and the independent model prediction. Also

shown in Table 1 are the model predictions using reflectance statistics derived from the Run 07 HYDICE data. These results are almost identical to the statistics obtained from the Run 07 data and confirm the model propagates the reflectance statistics through the system effects in a similar manner as the real atmosphere, sensor, and processing algorithms.

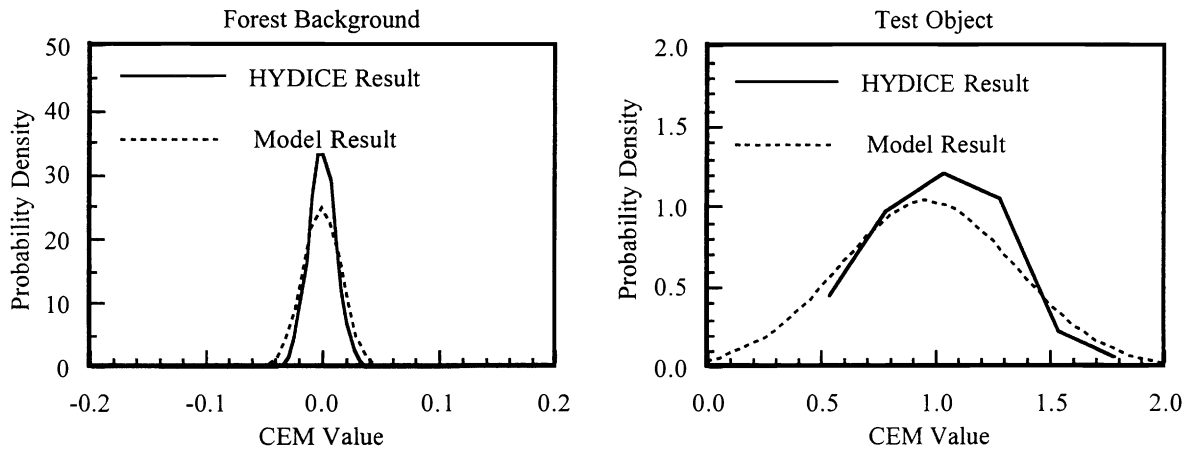


Figure 2. Model predictions of the CEM density functions using reflectance statistics derived from Run 05 compared to empirically derived histograms from the same area using Run 07 HYDICE data.

Table 1. Quantitative comparison of the mean and standard deviation of the CEM statistics for the HYDICE data and the model forecasts.

	HYDICE Run 07 Data	Model Run 05 Refl.	Model Run 07 Refl.
Target CEM Mean (θ_T)	1.000	0.963	0.969
Target CEM Standard Deviation ($\sigma_{\theta T}$)	0.299	0.386	0.290
Background CEM Mean (θ_B)	0.000	0.001	0.000
Background CEM Standard Deviation ($\sigma_{\theta B}$)	0.012	0.016	0.012

4.3 Probability of detection

The validation of predicted detection and false alarm probabilities was also studied by simulating subpixel mixtures of the HYDICE data using a weighted combination of randomly selected test object pixels with randomly selected forest pixels. This was necessary because the test object occupied entire pixels in the HYDICE imagery and was easily separable from the forest background and it was desirable to obtain a range of detection probabilities. Figure 3 shows a comparison of the detection probabilities for two false alarm rates over a range of object subpixel fractions. The comparison is very good between the model and the forecast; however, the false alarm probabilities that were evaluated were very high because of the limited number of background pixels available in the data.

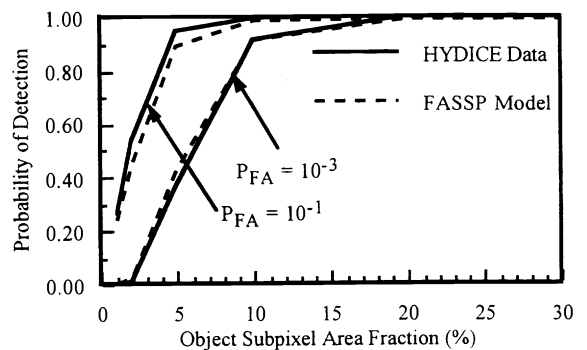


Figure 3. Comparison of the model forecast and empirically derived detection probabilities for two false alarm rate probabilities and the case of subpixel occurrences of the test object in the forest background. Subpixel HYDICE data were generated using a weighted linear combination of randomly selected target and background samples.

5. ANALYSIS EXAMPLE

This version of the FASSP model is designed to forecast the ability of a hyperspectral imaging system to find objects that are spatially unresolved, or subpixel. One potential application of subpixel detection is airborne Search and Rescue where the objective is to maximize search rate, while keeping detection probabilities high and false detection rates low. By using a hyperspectral imager coupled with an automated processor, significant surface areas could be covered rather quickly.

The example considered here is the case of the HYDICE sensor flying off a coast looking for an orange life vest in the ocean. Table 2 provides the details in the scenario. Two cases are considered to show the utility of the model to study sensitivity to environmental parameters: 1) clear conditions, no clouds, and 2) overcast conditions with clouds above the aircraft.

Figure 4 shows the results. As can be seen, the model predicts the life vest can be found even with only a small portion visible on the surface of the ocean. The reduced illumination in the overcast situation is seen to degrade the detection for small visible areas and requires more of the life vest be visible to achieve high detection rates.

Table 2. Life vest detection example scenario parameters.

Scenario Parameter	Setting
Target object class	Bright orange wet life vest (0.18 m ²)
Background class	Near coast ocean
Atmospheric haze model	Navy maritime
Wind speed	10 m/s => visibility = 30 km
Solar zenith angle	60°
Cloud cover	None; overcast at 2.4 km
Sensor	HYDICE
Sensor altitude	2 km
Ground pixel size	1 m
Sensor platform speed	100 m/s
Search area coverage	1.92 sq. km/minute (excluding turns)
Relative calibration error	0.5%
Sensor pixel integration time	5 msec
Atmospheric compensation	Linear correction
Spectral channels	121 from 0.5 – 1.3 μm, 1.5-1.7 μm, 2.0-2.3 μm
Detection algorithm	Constrained Energy Minimization using known spectrum
False detection rate threshold setting	1 per sq. km (10 ⁻⁶)

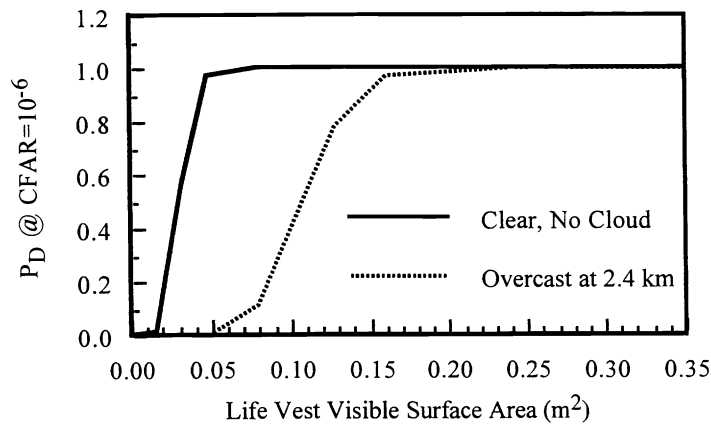


Figure 4. Example result for detecting a subpixel life vest floating on ocean.

6. SUMMARY

A model for predicting and analyzing the expected end-to-end performance of a spectroradiometric sensing system has been developed and has undergone preliminary validation. The theory behind the model, results of initial validation studies, and an example of its use have been presented.

The model uses the first and second order statistics of the spectral reflectance for surface objects and materials, and propagates them through the effects of the atmosphere, the sensor, and algorithmic transformations and operators to forecast the ability of a spectroradiometric sensing system to detect subpixel objects. The model has been used to study end-to-end performance of imaging spectrometer systems and their sensitivity to environmental and sensor parameters.

In the future, the model will be expanded to cover additional spectral ranges, sensor types, and processing algorithms, as well as the addition of measures of confidence to the model predictions. While the analytic formulation of the model may restrict the type of scenes, algorithms, and applications considered, the speed and robustness of this approach can provide great utility in system concept studies and near real-time operations support.

7. ACKNOWLEDGMENTS

The authors would like to acknowledge the support of the HYMSMO Program, and in particular Dr. Gregory Pavlin, the HYMSMO Technical Coordinator, for his support and interest in initiating this work. We would like to thank Mr. Larry Biehl, Purdue University, for his efforts in providing numerous spectral reflectance statistics files used in FASSP. Also, we would like to acknowledge Mr. Robert Basedow, Raytheon Optical Systems, Inc., for supplying detailed information to model the HYDICE sensor.

8. REFERENCES

1. J.P. Kerekes and D.A. Landgrebe, "Parameter Trade-Offs For Imaging Spectroscopy Systems," IEEE Transactions on Geoscience and Remote Sensing, vol. 29, no. 1, pp. 57-65, January 1991.
2. J.P. Kerekes, "Parameter Impacts on Hyperspectral Remote Sensing System Performance," *Hyperspectral Remote Sensing and Applications*, SPIE Vol. 2821, Denver, CO, August 5-6, 1996.
3. Schott, J.R., **Remote Sensing: The Image Chain Approach**, Oxford University Press, New York, NY, 1997.
4. A. Berk, L.S. Bernstein, D.C. Robertson, "MODTRAN: a moderate resolution model for LOWTRAN 7," GL-TR-89-0122, Spectral Sciences, Burlington, MA, 1989.
5. Y.J. Kaufman, "Atmospheric Effect on Spatial Resolution of Surface Imagery," Applied Optics, Vol. 23, No. 19, pp. 3400-3408, 1 October 1984.
6. L.J. Rickard, et al, "HYDICE: An Airborne System for Hyperspectral Imaging," Imaging Spectrometry of the Terrestrial Environment, SPIE Vol. 1937, 1993.
7. W.H. Farrand and J.C. Harsanyi, "Mapping the Distribution of Mine Tailings in the Coeur d'Alene River Valley, Idaho, Through the Use of a Constrained Energy Minimization Technique," Remote Sensing Environment, vol. 59, pp. 64-76, 1997.
8. S.J. Whitsitt and D.A. Landgrebe, "Error Estimation and Separability Measures in Feature Selection for Multiclass Pattern Recognition," LARS Publication 082377, Laboratory for Applications of Remote Sensing, Purdue University, West Lafayette, IN, August 1977.